# Hydrodeoxygenation of anisole to produce value-added products: ortho-, meta-, para-cresol

**Leonor Angélica Guerrero Zúñiga [1], Ana Cristina Ramirez-Gallardo [2], Maria Fernanda López Sánchez [2] and Isidoro Garcia-Cruz [2,*]**

[1] Research Management in Energy Efficiency and Biofuels. Mexican Petroleum Institute, Mexico City, Mexico.
[2] Research Management in Industrial Transformation. Mexican Petroleum Institute, Mexico City, Mexico.
* Corresponding author: igarcia@imp.mx

Received: May 9, 2025 Accepted: June 13, 2025 Published: June 18, 2025
DOI: https://doi.org/10.56845/rebs.v7i1.451

**Abstract:** This work presents a detailed study on the trans-methylation reaction using density functional theory (DFT), an advanced computational technique for analyzing and predicting molecular-level interactions. Trans-methylation is a crucial step in both catalytic and non-catalytic decomposition of methoxybenzene (anisole), with a special focus on processes generating free radicals and methyl-type carbocations through the cleavage of the methyl group. The study highlights that, in the presence of Brønsted-acid catalysts (such as HZSM-5), trans-methylation follows a specific mechanism involving dual electrophilic attack. This process begins with the interaction of the Brønsted acid proton with the oxygen atom in anisole, leading to carbocation substitution. This dual electrophilic attack mechanism is key as it explains how the catalyst alters reaction pathways to improve efficiency. Computational modeling of the reaction shows that the use of acidic catalysts drastically lowers the energy barriers of the investigated compounds, indicating that Brønsted acidity facilitates the reaction. In many cases, the reduction exceeds 40 kcal/mol, with the most significant decrease observed for ortho-cresol, where the energy barrier drops by approximately 60 kcal/mol. This demonstrates the significant influence of the catalyst on reaction kinetics. Both in catalytic and non-catalytic trans-methylation, there is a clear structural preference for the anisole molecule and its derivatives, such as cresols. The ortho and para positions are the most favored for substitution, especially when the substituents are oxygen-rich. This is because oxygenated substituents tend to lower energy barriers and enhance the reactivity of the aromatic ring, as seen in the decomposition of anisole into phenolic derivatives. This work demonstrates how the use of Brønsted-acid catalysts not only accelerates trans-methylation reactions but also alters the preferred reaction pathways, significantly reducing energy barriers. This opens the door to a deeper understanding and optimization of industrial processes involving the decomposition of aromatic compounds such as anisole. The production of benzene, toluene, and xylene (BTX), along with oxygenated aromatic compounds such as anisole and cresol, plays a significant role in various industrial applications, including the synthesis of polymers, resins, and fuel additives. While the manufacture of these aromatics is associated with environmental concerns—particularly emissions and toxic by-products—their contribution to sustainability can be enhanced through the adoption of greener synthesis pathways, improved catalytic efficiency, and the integration of renewable feedstocks. When aligned with circular economy principles and process intensification strategies, the production of BTX and oxygenated aromatics can support more sustainable chemical manufacturing frameworks.

**Keywords:** Hydrodeoxygenation; anisole; products; cresol

## Introduction

The large-scale production of benzene, toluene, and xylene (BTX) is essential for the national petrochemical industry. In this context, anisole is frequently used as a model compound to study the reactivity of lignin derivatives containing the methoxy functional group, given that anisole contains this as its sole functional group (Hurff & Klein, 1983). It has been observed that trans-methylation is the primary reaction in both the catalytic and non-catalytic decomposition of anisole, leading to the production of BTX compounds and phenol, as illustrated in Figure 1 (Qinglei *et al*., 2015) (Prasomsri *et al*., 2011) (Wang *et al*., 2014) (Cornella *et al*., 2013) (Mackie *et al*., 1989).

Catalytic hydrodeoxygenation (HDO) of anisole is a critical and efficient step to upgrade raw bio-oil, converting it into high-quality transportation fuels by reducing oxygen content and increasing calorific value. However, catalytic cracking can reduce the yield of liquid fuels and increase that of gaseous fuels, leading to carbon losses and the formation of short-chain hydrocarbons ($C_1$ to $C_4$). To produce high-performance fuels such as bio-jet fuel for aviation, it is essential to understand the HDO catalytic conversion process of biomass, which will enable better design of metallic catalysts and optimization of reaction conditions.

Given the complexity of raw bio-oil derived from biomass, the main objective of this work is to investigate the catalytic HDO reaction pathway of model compounds like anisole. First, the chemical and electronic structures of anisole and its

derivatives will be analyzed, as well as the structure of the HZSM5 zeolite-based catalyst, which has a significant impact on the conversion and selectivity of value-added products obtained from anisole degradation.

Previous studies have reported that the use of Ni supported on $TiO_2$-$ZrO_2$ (with 70 mol% $TiO_2$) as a catalyst enhances anisole HDO activity and selectivity toward hydrocarbons such as cyclohexane and benzene due to its improved dispersion and higher acidity. Additionally, it has been reported that bimetallic catalysts can increase anisole activity and modify its selectivity (Rios-Escobedo *et al*., 2022) (Zhang *et al*., 2014). Therefore, catalyst acidity is crucial, making zeolite-based catalysts an attractive alternative due to their significantly lower cost compared to metal-based catalysts such as Ni, Pd, and Ru.

This work proposes to study the reaction pathway of anisole using HDO catalysts, as shown in Figure 1. The reaction of anisole over HZSM5 zeolite-based HDO catalysts will be investigated to obtain value-added products such as cyclohexane, phenol, cyclohexene, toluene, and ortho-, meta-, and para-cresol. These products will be generated through different processes, including demethoxylation (DMO), hydrogenation (HYD), demethylation (DME), and alkylation (ALK). Alkylation will occur through the trans-methylation of the $CH_3^+$ - group in phenol, forming the ortho-, meta-, and para-cresol isomers.

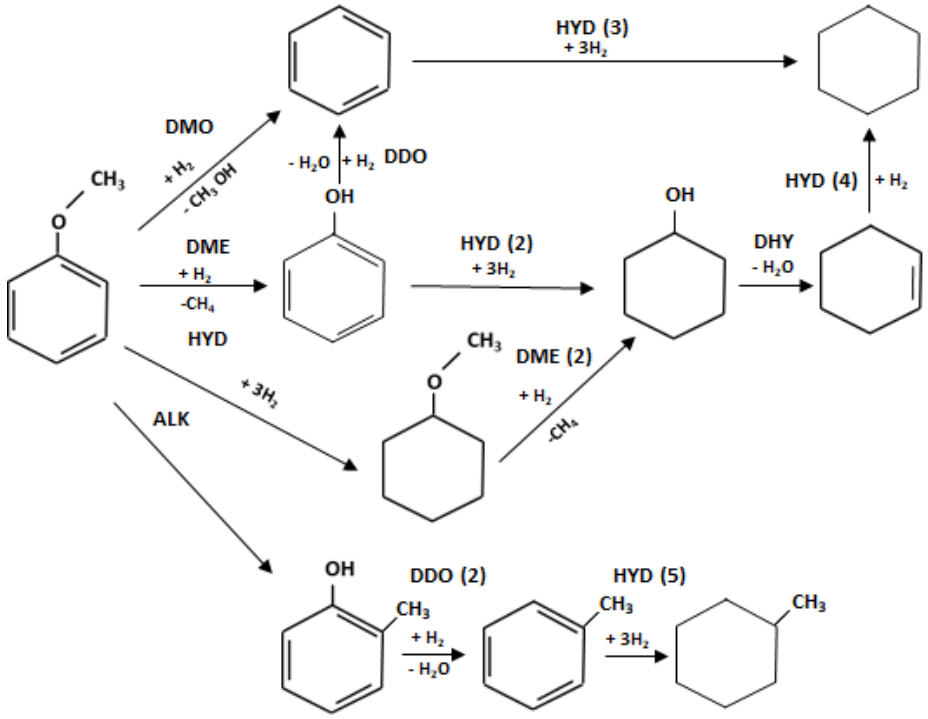


Figure 1. Reaction pathways of anisole over HDO catalysts

**Methodology for Calculations and Reaction Schemes**

Figure 1 and Figure 2 present the reaction scheme for the alkylation (ALK) of anisole, specifically the trans-methylation of the $CH_3^+$ - group at the ortho-, meta-, and para- positions of phenol, leading to the formation of ortho-, meta-, and para-cresol. The structures of anisole and its derivatives were optimized using density functional theory (DFT), employing the B3LYP functional (Lee *et al*., 1988) and the 6-31G(2df,p) basis set (Csonka *et al*., 2009) (Assary *et al*., 2010).

The B3LYP functional was selected because it is a widely used and well-parametrized reference functional for thousands of organic molecules, making it a reliable choice for this type of calculation. Additionally, the 6-31G(2df,p) basis set was chosen because oxygenated molecules such as anisole, phenol, and the HZSM5 zeolite contain oxygen atoms, which require the inclusion of atomic orbitals p, d, and f to account for the polarization and diffusion necessary for accurately describing the polarity of these systems.

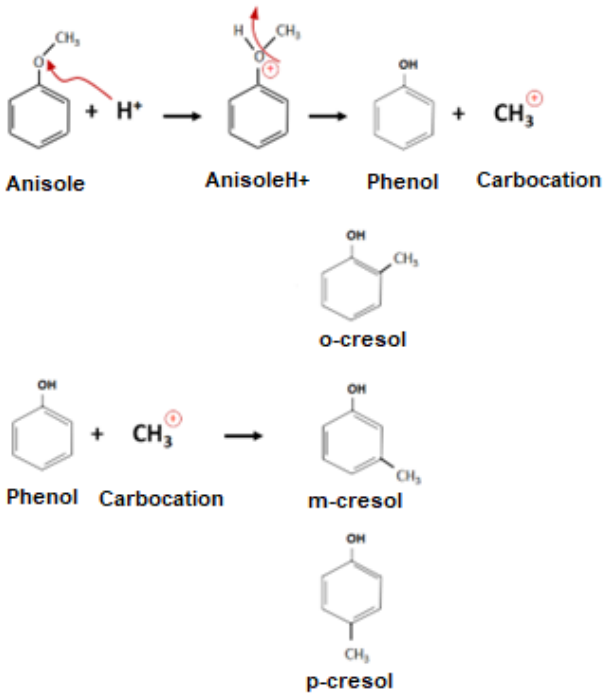


Figure 2. Reaction scheme of the methyl group ($CH_3^+$) trans-methylation from anisole to phenol to form ortho-, meta-, and para-cresol

To aid in understanding the optimized structures, Figure 3 provides the atom numbering in the structures and the representative species involved in the trans-methylation reaction for phenol formation. Meanwhile, Figure 4 shows the optimized structures of anisole and its derivatives obtained via DFT, which enable the formation of ortho-, meta-, and para-cresol.

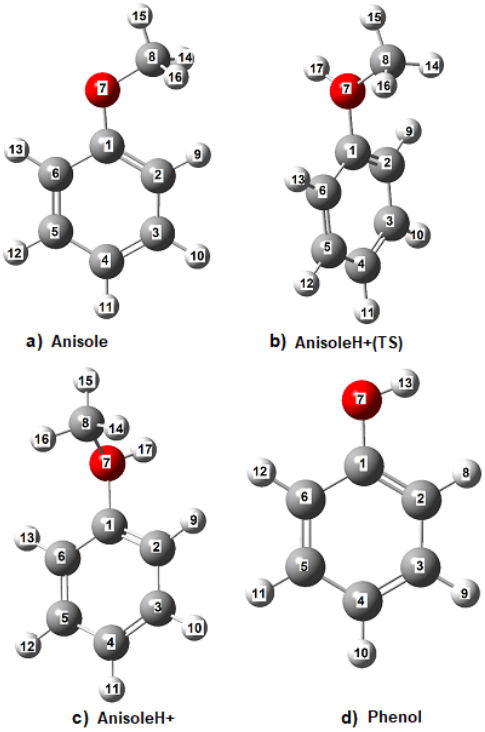


Figure 3. Numbering of the optimized geometry of the main components of the trans-methylation of anisole at the B3LYP/6-31G(2df,p) level

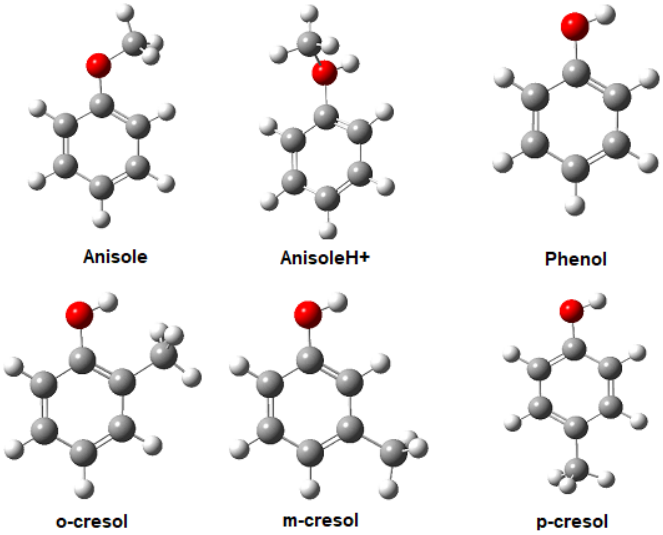


Figure 4. Optimized geometry of the main components of the trans-methylation of anisole at the B3LYP/6-31G(2df,p) level

During the optimization of anisole and its derivative structures using DFT, additional properties were calculated, including the total energy of the system, the energy of the highest occupied molecular orbital (HOMO), the energy of the lowest unoccupied molecular orbital (LUMO), and the energy gap between the HOMO and LUMO orbitals. Furthermore, Mulliken charges of all atoms in the system were determined, along with Fukui reactivity indices:

- f (+) for electrophilic substitutions,
- f (-) for nucleophilic substitutions,
- f (r) for radical-mediated substitutions.

These calculations provide a comprehensive understanding of the electronic structure and reactivity of anisole and its derivatives, facilitating the analysis of reaction pathways for the formation of value-added products.

**Results and Discussion**

The results section should include a precise description of the experimental results, a discussion of these results and their interpretation from the perspective of previous research and the hypotheses proposed. It is also necessary to mention possible future research.

The optimized structure of anisole and its derivatives obtained via DFT is shown in Figure 4. Table 1 details the bond distances and angles, while Table 2 presents the bond orders (B.O.), and Table 3 displays Mulliken electronic charges, as well as the Fukui reactivity indices calculated in this work and compared with those reported in the literature by Zhang *et al*. (2017). Finally, Figure 5 and Table 4 present the reaction barriers in kcal/mol for the trans-methylation reaction of anisole.

Table 1. Bond distance (in Å), bond angle, and dihedral angle (in °) of the optimized structures of anisole and its derivatives obtained at the B3LYP/6-31G(2df,p) level

| | **Anisole, A** | **AH(TS)** | **$AH^+$** | **Phenol** |
|---|---|---|---|---|
| | | **Bond distances (Å)** | | |
| $C_1$-$O_7$ | 1.362 | 1.461 | 1.474 | 1.364 |
| $C_8$-$O_7$ | 1.414 | 1.484 | 1.495 | |
| $C_1$-$C_2$ | 1.397 | 1.381 | 1.381 | 1.396 |
| $C_1$-$C_6$ | 1.401 | 1.381 | 1.379 | 1.396 |
| | | **Bond angles (°)** | | |
| $C_1C_7C_8$ | 118.21 | 123.37 | 117.86 | 109.01 |
| | | **Dihedral angles (°)** | | |
| $C_2C_1O_7C_8$ | 179.98 | 89.81 | 97.82 | 179.91 |

*1. Optimized Structure of Anisole and Its Derivatives*

The optimized geometry of anisole (A) using DFT reveals that the $C_1$-$O_2$ bond distance is 1.362 Å. In the transition state structure AH(TS), this distance increases to 1.461 Å, while in the protonated anisole $AH_+$ it is 1.474 Å, and in phenol, it is 1.364 Å. The $C_8$ - $O_7$ bond distance in anisole is 1.414 Å; in AH(TS) it increases to 1.484 Å, and in AH+ it is 1.449 Å. The $C_1$ - $C_2$ bond distance in anisole is 1.397 Å, reducing to 1.381 Å in both AH(TS) and $AH^+$, and it is 1.396 Å in phenol. On the other hand, the $C_1$ - $C_6$ bond distance in anisole is 1.401 Å; in AH(TS) it is 1.381 Å, in $AH^+$ it is 1.379 Å, and in phenol, it is 1.396 Å.

The $C_1$ - $O_7$ - $C_8$ bond angle in anisole is 118.21°, while in AH(TS) it increases to 123.37° and in $AH^+$ it is 117.86°. The dihedral angle $C_6C_1O_7C_8$ in anisole is 179.98°, but in AH(TS) it significantly decreases to 89.81°, and in $AH_+$ it is 97.82°, as detailed in Table 1. Although the bond distances and angles undergo some adjustments, no significant changes are observed in the optimized geometry of anisole and its derivatives, except for the dihedral angle. In the optimized structure of anisole, the $CH_3O$- group is positioned at a dihedral angle of $C_2C_1O_7C_8$ of 180° in the plane of the benzene ring. In the transition state, this angle reduces to 90°, and in protonated anisole, it is nearly 98°, as shown in Table 1.
The geometric optimization of anisole and its derivatives shows that the aromatic ring structure remains resonant and highly stable. The main structural changes are observed around the $CH_3O$- group. The $C_8$ - $O_7$ distance is longer compared to the $C_1$ - $O_7$ distance, which facilitates the cleavage of the $C_8$ - $O_7$ bond to form the $CH_3^+$- radical and phenol. Since the $C_1$ - $O_7$ bond distance is slightly larger, this cleavage may be easier, leading to the formation of benzene and methanol. After the formation of phenol, the trans-methylation leads to the formation of ortho-, meta-, and para-cresol, as shown in Figure 2 and Figure 4.

*2. Bond order of anisole and protonated anisole*

Table 2 shows the bond order (B.O.) of anisole and its protonated version. It is observed that the $C_1$-$O_7$ bond has a B.O. of 0.67, while the $C_8$-$O_7$ bond has a B.O. of 0.52, both with lower values compared to the rest of the molecule. The average B.O. of the C-C bonds in anisole is 1.03, and that of the C-H bonds is 0.81. The $C_8$-$H_{15}$ bond has a B.O. of 0.83, higher than the average for C-H bonds, stabilizing the resonant structure of anisole by forming a dihedral angle $C_1$-$O_7$-$C_8$-$H_{15}$. This behavior is also observed in the protonated anisole, although the B.O. of $C_1$-$O_7$ and $C_8$-$O_7$ are lower, indicating that the structure is less stable and more reactive, which facilitates its decomposition to form phenol.

Table 2. Mulliken bond order (B.O.) of the anisole (A) molecule and the protonated anisole ($AH^+$) for the trans-methylation reaction estimated at the B3LYP/6-31G(2df,p) level

| Bond | B. O. Mulliken | B. O. Mulliken |
|---|---|---|
| | A | $AH^+$ |
| $C_1$-$C_2$ | 1.030 | 0.099 |
| $C_1$-$C_6$ | 1.032 | 1.024 |
| $C_1$-$O_7$ | 0.668 | 0.364 |
| $C_8$-$O_7$ | 0.515 | 0.333 |
| $C_2$-$C_3$ | 1.003 | 1.026 |
| $C_3$-$C_4$ | 1.030 | 1.012 |
| $C_4$-$C_5$ | 1.063 | 1.007 |
| $C_5$-$C_6$ | 1.032 | 1.012 |
| $C_2$-$H_9$ | 0.813 | 0.819 |
| $C_3$-$H_{10}$ | 0.824 | 0.834 |
| $C_4$-$H_{11}$ | 0.825 | 0.836 |
| $C_5$-$H_{12}$ | 0.821 | 0.836 |
| $C_6$-$H_{13}$ | 0.814 | 0.828 |
| $C_8$-$H_{14}$ | 0.798 | 0.803 |
| $C_8$-$H_{15}$ | 0.826 | 0.814 |
| $C_8$-$H_{16}$ | 0.799 | 0.809 |
| $O_7$-$H_{17}$ | ------ | 0.676 |

The C$sp^3$–O bond in the optimized structure of the anisole molecule, with a $C_8$-$O_7$ bond distance of 1.414 Å, is the weakest. This distance increases to 1.484 Å in the transition state structure AH(TS) and to 1.449 Å in the protonated anisole $AH^+$, indicating that it is a weak bond, making it easier for the anisole molecule to break, forming the $CH_3^+$ cation and phenol, as shown in Figure 2 and Table 1. In this case, $C_8$ corresponds to the $CH_3^+$ group, and $O_7$ is the oxygen atom of the methoxy group, suggesting that both non-catalytic and catalytic thermal decomposition of anisole preferentially begin at this site (Li *et al*., 2014). In the case of non-catalytic decomposition of anisole, when the $C_8$-$O_7$ bond in the anisole molecule breaks, a methyl radical is formed, which substitutes a hydrogen atom in a phenol molecule to produce ortho-, meta-, and para-cresol (Zhang *et al*., 2017). It is likely that substitutions by the $CH_3^+$ radical

preferentially occur at the ortho- and para- positions of the phenol molecule because these positions favor an electrophilic attack, according to the Fukui reactivity indices (+) (Table 3). In a previous experimental study from Assary *et al*. (2010), it was established that the formation of cresol at temperatures below 650 °C is favored during the non-catalytic decomposition of anisole. It is important to note that, since there is no stable compound or intermediate in non-catalytic trans-methylation reactions, it is likely that cresol is obtained through a one-step reaction.

Table 3. Mulliken charges and Fukui reactivity indices for the atoms of anisole and its derivatives for electrophilic attack (Fukui(-)), calculated at the B3LYP/6-31G(2df,p) level and compared with the literature values.

| **Anisole/Atom** | **Mulliken C. This work** | **Mulliken C.** (Assary *et al*., 2010) | **Fukui Index f(-)** (Assary *et al*., 2010) | |
|---|---|---|---|---|
| A | | | | |
| $C_1$ | 0.410 | 0.299 | 0.075 | |
| $C_2$ | -0.257 | -0.064 | 0.086 | |
| $C_3$ | -0.089 | -0.083 | 0.061 | |
| $C_4$ | -0.127 | -0.063 | 0.125 | |
| $C_5$ | -0.085 | -0.097 | 0.071 | |
| $C_6$ | -0.194 | -0.133 | 0.072 | |
| $O_7$ | -0.264 | -0.438 | 0.129 | |
| $C_8$ | -0.245 | 0.008 | 0.035 | |
| $H_9$ | 0.094 | 0.074 | 0.046 | |
| $H_{10}$ | 0.093 | 0.077 | 0.044 | |
| $H_{11}$ | 0.090 | 0.088 | 0.057 | |
| $H_{12}$ | 0.094 | 0.081 | 0.046 | |
| $H_{13}$ | 0.099 | 0.076 | 0.040 | |
| $H_{14}$ | 0.123 | 0.087 | 0.037 | |
| $H_{15}$ | 0.134 | 0.102 | 0.038 | |
| $H_{16}$ | 0.123 | 0.086 | 0.036 | |
| **$AH_+$** | **Mulliken C. This work** | **Mulliken C.** (Assary *et al*., 2010) | **Fukui Index f(-)** (Assary *et al*., 2010) | **Fukui Index f(-)** (Assary *et al*., 2010) |
| $C_1$ | 0.315 | 0.216 | 0.058 | 0.048 |
| $C_2$ | -0.212 | -0.099 | 0.038 | 0.134 |
| $C_3$ | -0.076 | -0.048 | 0.024 | 0.128 |
| $C_4$ | -0.090 | -0.046 | 0.085 | 0.059 |
| $C_5$ | -0.081 | -0.049 | 0.025 | 0.120 |
| $C_6$ | -0.175 | -0.069 | 0.046 | 0.142 |
| $O_7$ | -0.236 | -0.370 | -0.057 | 0.017 |
| $C_8$ | -0.278 | 0.006 | 0.138 | 0.017 |
| $H_9$ | 0.147 | 0.116 | 0.060 | 0.056 |
| $H_{10}$ | 0.163 | 0.126 | 0.070 | 0.056 |
| $H_{11}$ | 0.161 | 0.127 | 0.050 | 0.045 |
| $H_{12}$ | 0.164 | 0.128 | 0.071 | 0.055 |
| $H_{13}$ | 0.162 | 0.130 | 0.070 | 0.058 |
| $H_{14}$ | 0.210 | 0.151 | 0.050 | 0.017 |
| $H_{15}$ | 0.226 | 0.166 | 0.063 | 0.046 |
| $H_{16}$ | 0.217 | 0.161 | 0.050 | 0.016 |
| $H_{17}$ | 0.382 | 0.354 | 0.140 | 0.024 |

Continuation Table 3. Mulliken charges and Fukui reactivity indices for the atoms of anisole and its derivatives for electrophilic attack (Fukui(-)), calculated at the B3LYP/6-31G(2df,p) level and compared with the literature values.

| Phenol | Mulliken C. This work | Mulliken C. (Assary *et al*., 2010) | Fukui Index f(0) (Assary *et al*., 2010) | Fukui Index f(-) (Assary *et al*., 2010) |
|---|---|---|---|---|
| $C_1$ | 0.410 | 0.283 | 0.073 | 0.089 |
| $C_2$ | -0.251 | -0.074 | 0.105 | 0.089 |
| $C_3$ | -0.077 | -0.144 | 0.095 | 0.068 |
| $C_4$ | -0.130 | -0.072 | 0.102 | 0.136 |
| $C_5$ | -0.082 | -0.119 | 0.099 | 0.073 |
| $C_6$ | -0.184 | -0.091 | 0.100 | 0.083 |
| $O_7$ | -0.444 | -0.440 | 0.103 | 0.152 |
| H8 | 0.081 | 0.057 | 0.057 | 0.049 |
| H9 | 0.095 | 0.059 | 0.055 | 0.061 |
| $H_{10}$ | 0.092 | 0.071 | 0.056 | 0.048 |
| $H_{11}$ | 0.096 | 0.054 | 0.056 | 0.050 |
| $H_{12}$ | 0.102 | 0.058 | 0.055 | 0.048 |
| $H_{13}$ | 0.296 | 0.257 | 0.044 | 0.055 |

*3. Reaction barrier of anisole and its derivatives*

Figure 5 and Table 4 show the reaction barrier in kcal/mol for the formation of ortho-, meta-, and para-cresol from the HDO of anisole. As can be seen in Figure 5, the critical step is the large reaction barrier of over 170 kcal/mol to reach the transition state AH(TS). This reaction barrier decreases to 7 kcal/mol to form a highly reactive and unstable species, protonated anisole ($AH^+$). This unstable species is highly reactive and favors the formation of phenol through the elimination of the $CH_3^+$ group. After the formation of protonated anisole, the reaction barrier decreases to -87 kcal/mol to form phenol, a very stable molecule. This phenol can then react with the $CH_3^+$ group at the ortho-, meta-, and para-positions via the trans-methylation of the $CH_3^+$ group. The trans-methylation of $CH_3^+$ allows the formation of the respective cresol, with lower reaction barriers of -97 kcal/mol and -98 kcal/mol for ortho- and meta-cresol, and -100 kcal/mol for para-cresol. This small variation in the reaction barrier of ~3 kcal/mol for the formation of ortho-, meta-, and para-cresol could justify the earlier statement by the group of Zhang *et al*. (2016), that the formation of cresol can occur in a single step.

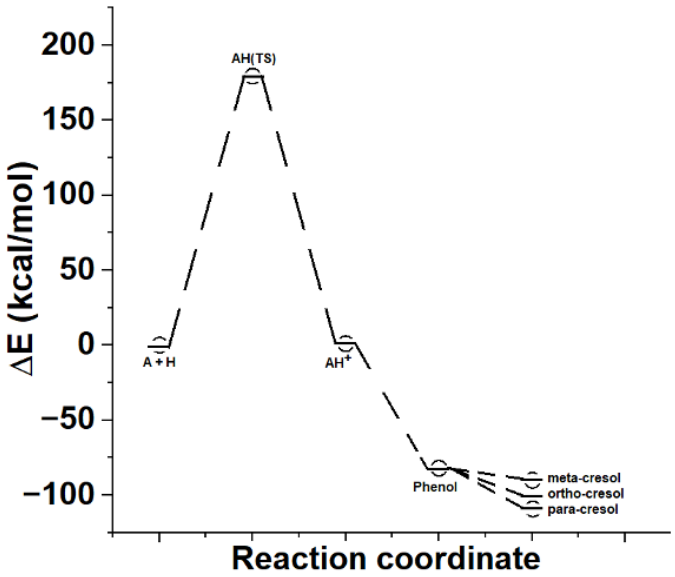


Figure 5. Energy barrier in kcal/mol for anisole to form phenol, ortho-, meta-, and para-cresol obtained with B3LYP/6-31G(2df,p)

Table 4. Energy barriers in kcal/mol for the HDO of anisole and the species involved in the reaction

| Molecules/Species | Ezpc | ΔH Enthalpy | ΔGFree energy |
|---|---|---|---|
| A+H | 0.00 | 0.00 | 0.00 |
| AH | 178.95 | 179.38 | 177.77 |
| $AH^+$ | 0.93 | 0.94 | 0.44 |
| Phenol | -80.96 | -82.06 | -71.61 |
| o-Cresol | -100.55 | -99.20 | -110.64 |
| m-Cresol | -100.22 | -98.99 | -109.64 |
| p-Cresol | -100.68 | -99.47 | -110.06 |

On the other hand, in the case of the catalytic decomposition of anisole over Brønsted acid sites of the HZSM5 zeolite, it has been established that the trans-methylation reaction is induced by a proton dissociated from the acidic site (-AlOH) and causes an electrophilic attack by one or more carbocations on anisole (Haw *et al*., 1989) (Richardson *et al*., 1990) (Munson *et al*., 1993) (Xu *et al*., 1994).

These studies state that the trans-methylation mechanism proceeds through carbocation transfers in the case of catalytic decomposition of anisole, as shown in Figure 2 and Figure 4.

The catalytic process of trans-methylation can be divided into two stages: i) the first consists of the cleavage or splitting of the methyl group $CH_3^+$ in the anisole molecule; the proton dissociated from the acid site of the catalyst causes an initial electrophilic attack on the oxygen atom of the anisole molecule, as shown in Figure 2 and Figure 4, and a methyl carbocation $CH_3^+$ is released. This $CH_3^+$ promotes a second electrophilic attack (Figure 2), and it is likely that this $CH_3^+$ group replaces a hydrogen atom at the ortho-, meta-, and para- positions of phenol, as shown in Figure 2 and Figure 4. The displaced free proton simultaneously interacts with the catalyst to regenerate the Brønsted acid site, thereby maintaining catalytic activity during the reaction. The transition-state species typically exist for a short time; however, the $CH_3^+$ bound to the active site during the trans-methylation process is a relatively stable structure (Figure 2), and carbocation substitution reactions via an electrophilic attack (Table 3) are favored as separate steps in catalytic trans-methylation. The mechanism in Figure 2 shows that the use of a Brønsted acid-type catalyst (the HZSM5 zeolite) replaces the one-step direct transfer reaction of $CH_3^+$ observed for the non-catalytic reaction with a two-step process (Zhu *et al*., 2010). The HZSM5-Anisole reaction mechanism also demonstrates the constant maintenance of acid sites in the catalyst by proton recovery throughout the reaction.

It is important to note that in both the catalytic and non-catalytic decomposition of anisole, the methyl group is transferred not only to phenol but also to other compounds such as benzene and toluene present in the reaction medium (Zhang *et al*., 2016). All trans-methylation processes start from the cleavage of the methyl group $CH_3^+$ from anisole.

*4. HZSM5 Zeolite and its Interaction with Anisole*

The Figure 6 shows the structure of the HZSM5 zeolite with four tetrahedral sites (4T). Structure A is the innermost ring of the HZSM5 zeolite structure with a Si/Al ratio of 30%, and it is the one modeled in this work. Structure B and Structure C represent the same zeolite, but with Si/Al ratios of 50% and 100%, respectively.

The geometry optimization result of the zeolite HZSM5 ring shows that the Mulliken atomic charges of the acidic hydrogens bonded to the O linked to an Al atom in a tetrahedral site and to a Si atom in the HZSM5 zeolite ring are very acidic, as shown in Table 5. The higher the charge on the hydrogen, the more acidic its character. In this work, the hydrogen atoms H(39), H(40), H(41), and H(42) in the zeolite HZSM5 ring structure are the most acidic hydrogens, which stabilize the negative charge of the 4T sites of the -AlOH anion, with H(42) being the most acidic hydrogen among all four tetrahedral sites with a charge of 0.368, followed by $H_{40}$ with 0.359, $H_{41}$ with 0.351, and finally $H_{39}$ with 0.345, as

seen in Table 5 and Figure 7. The most acidic tetrahedral site is where the anisole can be more easily activated in its interaction with the HZSM5 zeolite, and when the total HZSM5-zeolite-anisole interaction is reached, the protonated anisole or $AH_+$ is formed, favoring the formation of phenol and benzene.

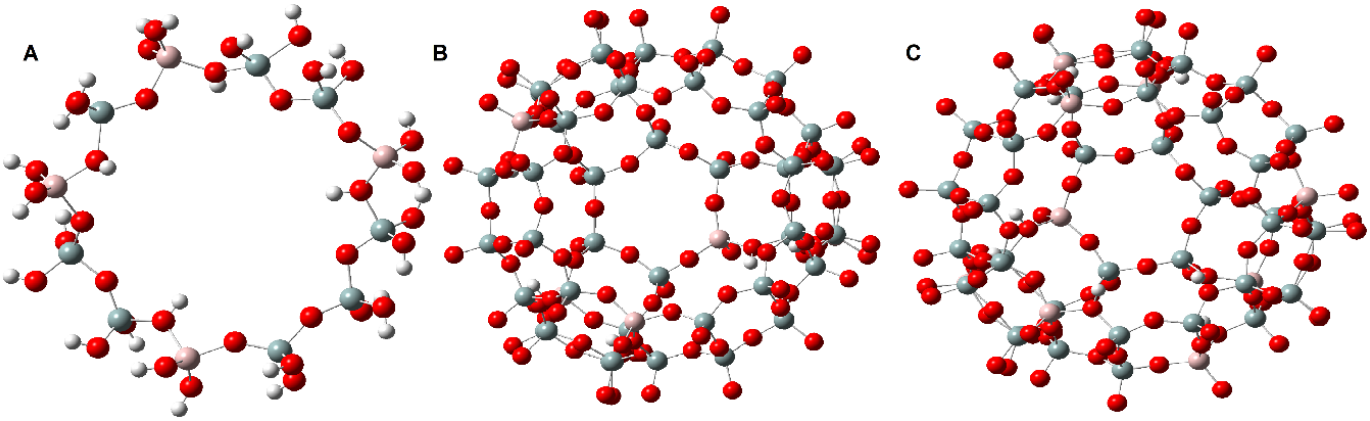


Figure 6. Models of HZSM5-type zeolites: A) Zeolite ring with four tetrahedral centers (4T); B) HZSM5 zeolite structure with a 50% ratio; C) HZSM5 zeolite structure with a 100% ratio. The O atom is colored red, the Si atom is gray, the Al atom is pink, and the H atom is white.

Table 5 Mulliken charges of the acidic hydrogens in the HZSM5 zeolite ring obtained at the B3LYP/6-31G(2df,p) level.

| Atom/H Position in the Ring | Mulliken charge |
|---|---|
| H(39) | 0.345 |
| H(40) | 0.359 |
| H(41) | 0.351 |
| H(42) | 0.368 |

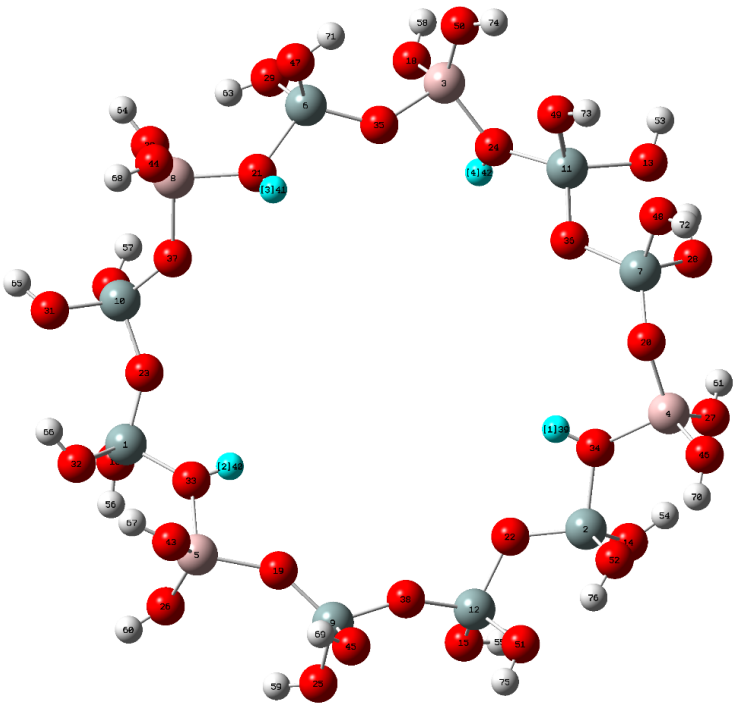

Figure 7. Structure of the HZSM5 zeolite ring optimized at the B3LYP/6-31G(2df,p) level. The atoms in light blue are the H atoms that stabilize the tetrahedral sites of -AlOH

## Conclusions

The results obtained with DFT indicate that the trans-methylation reaction is a crucial step in both the non-catalytic and catalytic decomposition of anisole. The cleavage of the $C_8$-$O_7$ bond leads to the formation of the $CH_3^+$ radical. In catalytic trans-methylation, the reactants interact with the Brønsted acid sites present in the HZSM5-based catalyst. This process is initiated by the electrophilic attack of the Brønsted acid proton on the oxygen atom of the anisole, followed by the substitution of the hydrogen with $CH_3^+$.

In this work, a dual electrophilic attack mechanism for catalytic trans-methylation is proposed. The reaction modeling, based on the proposed mechanism, shows that a catalyst with higher Brønsted acidity can significantly reduce the energy barrier for all the compounds investigated, due to changes in the reaction pathways. Most of the energy barriers for the evaluated trans-methylation reactions decrease by approximately 40 kcal/mol when considering the catalytic effect, with the greatest decrease observed in the case of ortho-cresol (around 60 kcal/mol).

Furthermore, both non-catalytic and catalytic trans-methylation of anisole exhibit a preference for the formation of phenol, with most of the species involved showing a preference for the para-phenol position, depending on the substituents. Non-catalytic transmethylation to oxygen-rich substituted compounds generally presents lower energy barriers. In the catalytic decomposition of anisole, the presence of oxygen-rich substituents also enhances the reactivity of the ring, especially for phenolic compounds at the para- position. The lowest energy barrier was observed in the case of trans-methylation to the para- position of phenol, with the barrier to form para-cresol being approximately 102 kcal/mol.

**Acknowledgments and Funding:** The authors extend their sincere appreciation to the Mexican Petroleum Institute (IMP) for its financial support through research grant D.62026. The computational resources fundamental to this work were generously provided by the National Supercomputing Center at IPICyT (Potosino Institute of Scientific and Technological Research), under project allocation TKII-E-0424-I-170424-26/PR-33: *Mechanistic modeling of molecular disintegration in mixtures of unconventional feeds in FCC units*. The authors gratefully acknowledge the valuable infrastructure and expert technical assistance offered by the Supercomputing Center team, which played a pivotal role in the successful execution of this research.

**Declaration of competing interest:** The authors declare that they have no financial or personal conflicts of interest that could have influenced the results or interpretation presented in this manuscript. All contributions to this work were conducted with full scientific independence and integrity.

**Author contributions:** G. C.-I. and R. G.-A. C. contributed equally to the conceptual design of the study, performed the computational analyses, interpreted the data, and were primarily responsible for drafting and revising the manuscript. G. Z.-L. A. and L. S.-M. F. were responsible for providing key experimental materials, coordinating laboratory operations, designing the methodology for data acquisition, and supervising the overall research process. All authors reviewed and approved the final version of the manuscript and agree to be accountable for all aspects of the work.

## References

Assary, R. S., Redfern, P. C., Hammond, J. R., Greeley, J., & Curtiss, L. A. (2010). Computational Studies of the Thermochemistry for Conversion of Glucose to Levulinic Acid. *The Journal of Physical Chemistry B*, 9002-9009. https://doi.org/10.1021/jp101418f

Cornella, Cornella, J., Gómez-Bengoa, E., & Martin, R. (2013). Combined Experimental and Theoretical Study on the Reductive Cleavage of Inert C-O Bonds with Silanes: Ruling out a Classical Ni(0)/Ni(II) Catalytic Couple and Evidence for Ni(I) Intermediates. *Journal of the American Chemical Society*, 1997-2009. https://doi.org/10.1021/ja311940s

Csonka, Csonka, G. I., French, A. D., Johnson, G. P., & Stortz, C. (2009). Evaluation of Density Functionals and Basis Sets for Carbohydrates. *Journal of Chemical Theory and Computation*, 679-692. https://doi.org/10.1021/ct8004479

Haw, J. F., Richardson, B. R., Oshiro, I. S., Lazo, N. D., & Speed, J. A. (1989). Reactions of propene on zeolite HY catalyst studied by in situ variable temperature solid-state nuclear magnetic resonance spectroscopy. *Journal of the American Chemical Society*, 2052-2058. https://doi.org/10.1021/ja00188a016

Hurff, S. J., & Klein, M. T. (1983). Reaction pathway analysis of thermal and catalytic lignin fragmentation by use of model compounds. *Industrial & Engineering Chemistry Fundamentals*, 426-430. https://doi.org/10.1021/i100012a012

Lee, C., Yang, W., & Parr, R. G. (1988). Development of the Colle-Salvetti correlation-energy formula into a functional of the electron density. *Physical Review B*, 785. https://doi.org/doi.org/10.1103/PhysRevB.37.785

Li, G., Li, L., Jin, L., Tang, Z., Fan, H., & Hu, H. (2014). Experimental and Theoretical Study on the Pyrolysis Mechanism of Three Coal-Based Model Compounds. *Energy & Fuels*, 980-986. https://doi.org/10.1021/ef402273t

Mackie, J., Doolan, K., & Nelson, P. (1989). Kinetics of the thermal decomposition of methoxybenzene (anisole). *The Journal of Physical Chemistry*, 664-670. https://doi.org/10.1021/j100339a033

Munson, E. J., Xu, T., & Haw, J. F. (1993). In situ nuclear magnetic resonance study of allyl alcohol conversion on zeolites: evidence for an allyl cation intermediate. *Journal of the Chemical Society, Chemical Communications*, 75-76. https://doi.org/10.1039/C39930000075

Prasomsri, T., To, A. T., Crossley, S., Alvarez, W. E., & Resasco, D. E. (2011). Catalytic conversion of anisole over HY and HZSM-5 zeolites in the presence of different hydrocarbon mixtures. *Applied Catalysis B: Environmental*, 204-211. https://doi.org/10.1016/j.apcatb.2011.05.026

Qinglei, M., Honglei, F., Huizhen, L., Huacong, Z., Zhenhong, H., Zhiwei, J., . . . Buxing, H. (2015). Efficient Transformation of Anisole into Methylated Phenols over High-Silica HY Zeolites under Mild Conditions. *ChemCatChem*, 2831-2835. https://doi.org/10.1002/cctc.201500479

Richardson, B. R., Lazo, N. D., Schettler, P. D., White, J. L., & Haw, J. F. (1990). Reactions of butadiene in zeolite catalysts by in situ variable-temperature solid-state nuclear magnetic resonance spectrometry. *Journal of the American Chemical Society*, 2886-2891. https://doi.org/10.1021/ja00164a007

Rios-Escobedo, R., Ortiz-Santos, E., Colín-Luna, J., Díaz de León, J., del Angel, P., Escobar, J., & de los Reyes, J. (2022). Anisole Hydrodeoxygenation: A Comparative Study of Ni/TiO2-ZrO2 and Commercial TiO2 Supported Ni and NiRu Catalysts. *Topics in Catalysis*, 1448-1461. https://doi.org/10.1007/s11244-022-01662-x

Wang, K., Dong, X., Chen, Z., He, Y., Xu, Y., & Liu, Z. (2014). Highly selective synthesis of para-cresol by conversion of anisole on ZSM-5 zeolites. *Microporous and Mesoporous Materials*, 61-65. https://doi.org/10.1016/j.micromeso.2013.11.007

Xu, T., Zhang, J., Munson, E. J., & Haw, J. F. (1994). A report of a persistent allyl cation on H-ZSM-5 zeolite was due to propanal. *Journal of the Chemical Society, Chemical Communications*, 2733-2735. https://doi.org/10.1039/C39940002733

Zhang, J., Fidalgo , B., Shen, D., Xiao, R., & Gu, S. (2016). Mechanism of transmethylation in anisole decomposition over HZSM-5: Experimental study. *Journal of Analytical and Applied Pyrolysis*, 323-331. https://doi.org/10.1016/j.jaap.2016.09.009

Zhang, J., Fidalgo, B., Kolios, A., Shen, D., & Gu, S. (2017). The mechanism of transmethylation in anisole decomposition over Bronsted acid sites: density functional theory (DFT) study. *Sustainable Energy Fuels*, 1788-1794. https://doi.org/10.1039/C7SE00280G

Zhang, Zhang, X., Long, J., Kong, W., Zhang, Q., Chen, L., . . . Li, Y. (2014). Catalytic Upgrading of Bio-oil over Ni-Based Catalysts Supported on Mixed Oxides. *Energy & Fuels*, 2562-2570. https://doi.org/10.1021/ef402421j

Zhu, X., Mallinson, R. G., & Resasco, D. E. (2010). Role of transalkylation reactions in the conversion of anisole over HZSM-5. *Applied Catalysis A: General*, 172-181. https://doi.org/10.1016/j.apcata.2010.03.018